Atmospheric transmission and thermal background emission in the mid-infrared at Mauna Kea

A Otárola[1], M Richter[2], C Packham[3] and M Chun[4]

1111 South Arroyo Parkway, Pasadena, CA 91105, USA
1 Shields Ave, Davis, CA 95616, USA
1, UTSA Circle, Dept. of Physics & Astronomy, UTSA, San Antonio, TX 78249, USA
640 N. A'ohoku Place, Hilo, HI 96720, USA

E-mail: aotarola@tmt.org

Abstract.

We present results of a preliminary study intended to quantitatively estimate the atmospheric transmission and thermal background emission in the mid-infrared (MIR), 7 μm - 26 μm, at the 13N TMT site in Mauna Kea. This is in the interest of supporting the planning of MIR instrumentation for the posible second-generation of astronomical instruments for the Thirty Meter Telescope (TMT) project. Mauna Kea, located at high altitude (4,050 m above sea level), enjoys natural conditions that make it an outstanding location for astronomical observations in the mid-infrared. The goal of this work is to produce a dataset and model that shows the atmospheric transmission and thermal emission for two cases of precipitable water vapor (PWV), a low value of 0.3 mm, and at 1.5 mm which represent near median conditions at the site. Besides, and driven by the interest of the MIR community to exploit the daily twilight times, we look at the specific atmospheric conditions around twilight as a function of season. The best conditions are found for cold and dry winter days, and in particular the morning twilight offers the best conditions. The analysis of PWV data, shows the median value for the site (all year conditions between 6:00 PM and 7:30AM) is 1.8 mm and that periods of water vapor lower than 1.0 mm are common, these supports the opportunity and discovery potential of the TMT project in the mid-infrared bands.

1. Introduction

The Thirty Meter Telescope (TMT) Project contemplates the development of MIR instrumentation (imaging and spectroscopy) for its second generation instruments. In general, the MIR allows to probe the dynamics and chemistry of regions highly obscured by surrounding dust, such as is found in the central region of galaxies and star forming regions. Observations in the MIR enable interesting science, such as: evolution of gas and chemistry in protoplanetary discs, the study of star and planet evolution (kinematics and physical & chemical evolution), study of accretion and outflows around protostars, characterization of exoplanet atmospheres as well as potential for the detection of biomarkers from transmission spectral studies in exoplanet atmospheres, evolutionary connections of black holes & galaxies. Also, the MIR enables the study of moderate redshifted objects, the [SIV] line (10.5 μm) is an excellent substitute with superior ground-based sensitivity instead of the [OIV] line. In our solar system, near- and mid-infrared astronomy allows the study of the thermal structure, chemistry, photo-chemical products, and dynamics in the thick planetary atmospheres of the giant gaseous plane [1].

One important limiting factor in the observation at MIR wavelengths (7 μm to 26 μm) from ground-based observatories is the water vapor in our atmosphere. This arises from the water vapor absorption, due to the complex ro-vibrational spectrum of water vapor molecules, and added noise in the detectors from atmospheric thermal emission [2]. Consequently, the biggest difference between the MIR and visible spectral regions, from the point of view of instrument design, is the large amount of thermal background radiation in the mid-infrared [3].

The overall effect of such limiting factors vary strongly from site to site.

Here we model the atmospheric transmission and thermal background emission in the MIR at the 13N site; the place chosen for the construction and operation of the Thirty Meter Telescope [4]. Ultimately, once including information on the thermal emission of the telescope optics (3 mirrors), that of the MIR adaptive optics system as well as the thermal emission in the optics of a potential MIR instrument, a more general model will be obtained to estimate the signal-to-noise ratio of astronomical observations in this spectral band and estimate the performance of the MIR camera and spectrograph when operated as part of the TMT suite of instruments.

Other goals of this study are to summarize the cumulative functions and statistics of precipitable water vapor at the 13N site, as well as provide information on the median conditions of surface temperature and ground-layer atmospheric turbulence at the site. All these parameters are relevant for the modeling of atmospheric transmission in the mid- and far-infrared, especially in the Q (17 μm to 26 μm) and Z (28 μm to 40 μm) spectral bands. The N mid-infrared band 7.0 μm to 14.5 μm isn't that sensitive to the water vapor levels in the atmospheric column, but the wings of this spectral band are limited by atmospheric O_3 in the middle of the band while CH_4 is the major feature at the short end, and CO_2.

Section 2 presents the datasets and methodology used in this study, section 3 shows the main results for the site, in terms of main atmospheric characterization and the atmospheric transmission and thermal background emission in the (7 μm to 26 μm) spectral region, and finally Section 4 includes the main conclusions of this work.

2. Datasets & Methodology

2.1. Datasets

The most relevant variables on which information is needed to model the atmospheric transmission and thermal background emission in the MIR includes the atmospheric temperature and absolute humidity. The best conditions for astronomical observations in the mid- far-infrared, specially for the Q infrared band are obtained, from very high elevation sites which are cold and dry [5]. The 13N site in Mauna Kea, with its altitude of 4,050 m above sea level, is one of the driest places [6] and is already hosting MIR instruments such as TEXES [3] used in the Gemini North and the IRTF telescopes and COMICS [7] at the Subaru telescope.

For characterization of the PWV of the 13N site, we used PWV data derived from the monitoring of optical depths at 225 GHz (τ_{225}) using a tipping radiometer[1] performed at the Caltech Submillimeter Observatory (CSO) in Mauna Kea and nearby the 13N TMT site[2]. The relation used in this study for deriving PWV from τ_{225} is $PWV(mm) = 21.422 \times \tau_{225} - 0.2950$[3].

Also important is the vertical distribution of absolute humidity in the atmosphere, since low-level water vapor is responsible for larger collisional broadening of the atmospheric absorption lines, and so is a source of higher thermal emission. For the vertical profile of absolute humidity we learned the median profile, for winter conditions at Mauna Kea, from radiosonde soundings launched from the PHTO 91285 (HILO) National Weather Service station[4].

[1] ALMA Memo Series #49, http://science.nrao.edu/facilities/alma/aboutALMA/Technology/ALMA_Memo_Series
[2] 225 GHz optical depth database at Caltech Submillimeter Observatory, http://cso.caltech.edu/tau/
[3] S Radford, Private Communication
[4] Radiosonde soundings database, Hilo station ID is PHTO: http://weather.uwyo.edu/upperair/sounding.html

The surface temperature data come from the site study[5] conducted by the TMT site testing team in the period 2004-2008 [4].

2.2. Methodology

PWV at the exact location of the 13N site ($\phi = 19.8339^o$ N; $\lambda = 155.4810^o$ W), was derived from 2-minute averages of surface measurements of air temperature (T) and relative humidity (RH) obtained during the TMT site testing campaign in the period 2005/06/29 - 2007/12/31. For the exact procedure for estimating PWV from surface weather data see [6].

As for the determination of the atmospheric radiance for the MIR, the following steps were performed:

The radiosonde soundings, obtained from the HILO National Weather Station, were used to obtain a typical profile of atmospheric temperature and absolute humidity for the Mauna Kea site. Best conditions of observations in the MIR are achieved in winter time, at low PWV and cold atmospheric temperatures. The profiles, in the upper troposphere and up to 90km above sea level, were complemented with data from the US standard atmosphere for winter conditions [8]. The absolute humidity profile was normalized, and subsequently adjusted for any desired level of integrated precipitable water vapor.

A line-by-line, layer-by-layer radiative transfer model, implemented in Matlab, making use of HITRAN [9] spectral line information, was used to derive the layer and total atmospheric transmission spectra. The radiative transfer model includes the atmospheric composition as shown in Table 1 of [5], and was run for two cases of PWV, a very dry case (with PWV=0.3 mm) and a near median condition (PWV=1.5 mm).

The physics formulation of the radiative transfer model is out of the scope of this conference paper. However, suffice is to say that the model output produces the absorption spectra ($\alpha_{mol_j,layer_i}$), for the following molecular species mol_j =N_2, O_2, CO_2, CH_4, CO, N_2O and H_2O, and for each and all of the atmospheric layers ($layer_i$) defined by the temperature and water vapor profiles.

The transmission $Tr_{layer_i}(\lambda)$, of each of the atmospheric layers is obtained from the first expression in the set of equations shown below. The layer emissivity $\epsilon_{layer_i}(\lambda)$, for each corresponding layer, is obtained from the complement to unity as follows: $\epsilon_{layer_i}(\lambda) = 1 - Tr_{layer_i}(\lambda)$. The radiance of each layer, as a function of wavelength, is obtained from multiplying the layer's emissivity and the Planck energy density function evaluated at the physical temperature of the layer. Finally, the total atmospheric radiance is the sum of all the atmospheric layers. This form of computing the overall atmospheric radiance is more accurate than simply multiplying the emissivity of the lowest most atmospheric layer by the corresponding Planck density function.

$$\begin{aligned}
&\mathrm{Tr}_{layer_i}(\lambda) = \exp(\sum_{mol_j} \alpha_{mol_j,layer_i} \cdot dH_{layer_i}) \\
&Rsky_{layer_i}(\lambda) = \epsilon_{layer_i}(\lambda) \cdot \{\tfrac{2\pi hc^2}{\lambda^5} \tfrac{1}{exp(\frac{hc}{\lambda k T_i})-1}\} \\
&Rsky_{total}(\lambda) = \sum_{i=1}^{N} R_{layer_i}(\lambda) \quad (1)
\end{aligned}$$

Multi-annual time series of precipitable water vapor data, surface temperature and surface turbulence data was analyzed to obtain an statistical characterization of those parameters, in terms of hourly medians, for the course of the day. This allow us to obtain a perspective on

[5] TMT Site testing database: http://sitedata.tmt.org

how those parameters change through the day and learn their behavior in the period from the afternoon twilight, through the night and into the morning twilight. The information presented this way will bring light to the proposal of the MIR community about using one or two hours of observing time at around morning twilight for additional observing time.

3. Results & Analysis

3.1. Atmospheric transmission and atmospheric radiance in the mid-infrared

Table 1 (insert to Fig. 1) shows the statistical percentiles of PWV out of 352534 values of PWV (only data in the period 6:00 PM to 7:30 AM local time are used for the statistics) and Fig. 1 shows the cumulative function of PWV for every month in 2012. The cumulative functions in Fig. 1 illustrate that, when looking at the driest conditions, the driest period is that of January through April, as shown by the first quartile with a PWV $\leq$ 0.75 mm. These are also cold months, as shown in Fig. 4, and together low precipitable water vapor in the atmospheric column and low low-level temperatures, are the best combination for astronomical observations in the MIR bands.

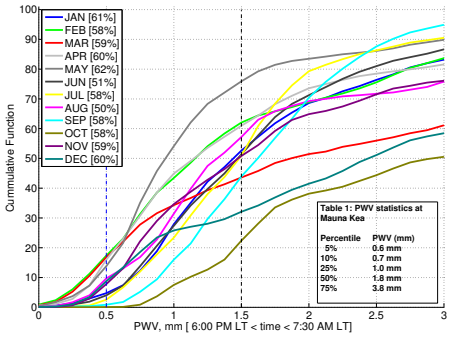

Figure 1. PWV monthly cumulative functions (2012).

In particular, we computed the atmospheric irradiance, following the procedure outlined in the previous section, for two conditions of PWV: a very dry atmosphere, with PWV=0.3mm, and a near median condition with PWV=1.5 mm. Figure 2(a) shows the atmospheric transmission, while Fig. 2(b) shows the atmospheric irradiance. The atmospheric molecular species responsible for the main absorption bands are CH_4 below 8 μm, O_3 in the vicinity of 9 μm, CO_2 with a strong absorption band in the range 13 μm - 17 μm, and various absorption lines resulting from the vibrational spectrum of the H_2O molecule in the range from 18 μm to 30 μm. The N band shows little change with water vapor, but the transmission of the various spectral windows beyond 18 μm show an increasingly dependance on the water vapor content.

The information shown in Fig. 2(b) can be used to compute the noise, at a particular spectral window in the detector of a mid-infrared instrument, that originates in the thermal emission of the atmosphere. For instance, the lowest radiance levels in the region around 11.5 μm wavelength is of about 2×10^{-7} W sr^{-1} cm^2 μm^{-1} (or 1.16×10^{-16} W arcsec^{-2} cm^2 μm^{-1}).

3.2. A proposal for using the twilight time for observations in the mid-infrared bands

The MIR community has proposed that one way of maximizing the scientific output of the telescope could be done by using about 1-2 hours of observing time available in the evening and/or morning twilights. One example of such approach is the use of TEXES instrument at the IRTF in Mauna Kea. This has motivated the community to look at how the PWV, air temperature and turbulence behaves as a function of time through the day at sites of interest.

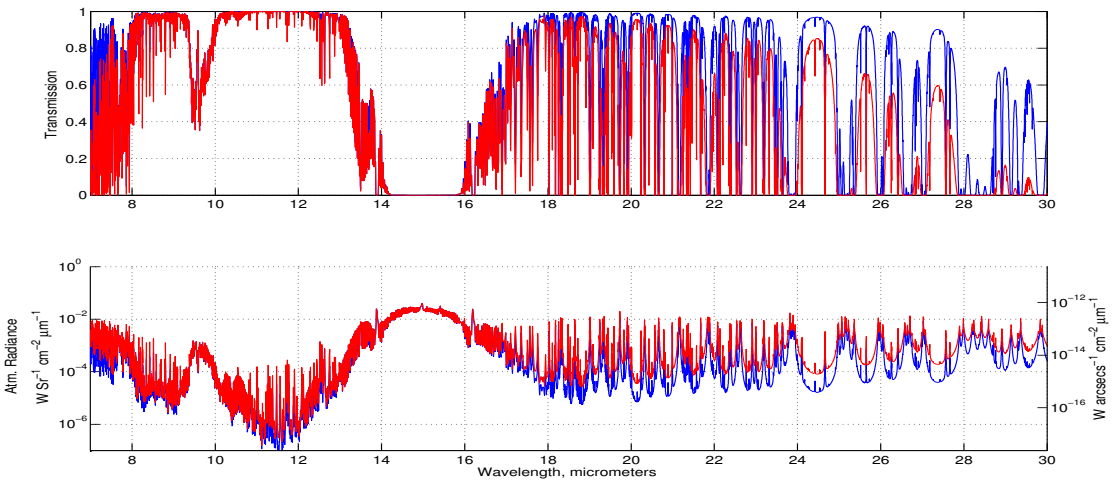

Figure 2. a) Atmospheric Transmission Spectrum for two cases of PWV (0.3 mm in blue, and 1.5 mm in read) and for a winter temperature profile condition; b) Atmospheric Radiances for the same cases of PWV.

In particular, for the 13N site, the PWV data measured at the CSO site in the period of four years (204-2007), and inferred from observations of optical depth at 225 GHz, was analyzed to compute the percentage of the time when the PWV was at a given PWV level as a function of local time. The calculations were done computing the fraction of the number of cases when the PWV falls in a bin of 0.125 mm size (as a function of absolute PWV level) for a time interval of 15 minutes (through the day) with respect to the total number of observations performed within that time window in the 4 years of data. Such map is therefore a robust way to show what is the statistical behavior of PWV as a function of time of day. The results are shown in Fig. 3 together with the 25%, 50% and 75% quartiles. This clearly illustrate that the maximum of PWV levels is about 0 hours UT (2:00 PM LT). The trend shows that PWV levels decreases through the afternoon reaching the lowest levels at about 5 UT (7:00 PM LT) and it remains at low levels until about 19 UT (9:00 AM LT). This is an interesting result. First, PWV in the atmospheric column is dominated by advection of air masses of different PWV content, but at low levels there is also a contribution from evaporation and/or sublimation depending on season and soil moisture condition. This in itself might lead to some variability as a function of time of day. However, this result is likely also the effect of a near surface temperature inversion that changes in altitude during daytime, when subsiding then it traps the water vapor below and at some point the temperature inversion goes below the altitude of the CSO site, allowing a dryer atmospheric column.

Another important parameter is near surface atmospheric temperature. For this purpose, the monthly median, as a function of time of day, was computed from data obtained at the 13N site during the TMT site testing campaign in 2006. The results are shown in Fig. 4. The daily and monthly temperature cycles are evident, with the coldest months being January, February and March. Regarding the daily cycle, the near surface atmosphere cools down by radiative processes starting with sunset and reaching the lowest temperature (near equilibrium) by 15:00-16:00 UT (5:00 - 6:00 LT). The temperature starts warming up with the sunrise. Stable temperature conditions are found during the morning twilight.

In this analysis we have also looked at the behavior of near surface atmospheric turbulence. The turbulence strength (C_n^2), was derived from fast temperature fluctuations observed with a Sonic anemometer operating at 30 Hz. The monthly median of C_n^2 as a function of time of

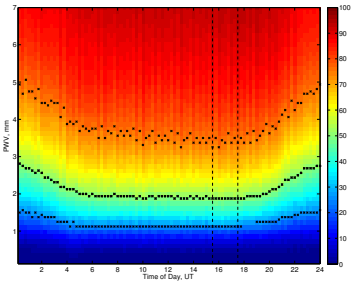

Figure 3. PWV probability of occurrence matrix as a function of time (UT) at Mauna Kea (CSO site).

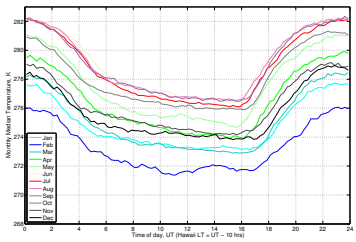

Figure 4. Monthly medians of near surface air temperature at the 13N site in Mauna Kea.

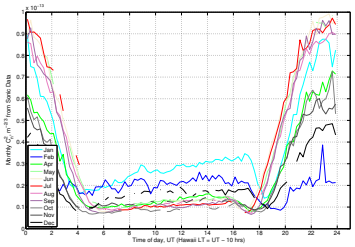

Figure 5. 2006 Monthly medians of surface turbulence strength (C_n^2)) at Mauna Kea.

day (with a time resolution of 15 min) are shown in Fig. 5. Again, the lowest conditions of near surface turbulence are observed towards the end of the night into the morning twilight, this as a result of lower variability in the air index of refraction due to the fact the atmospheric temperature by this time of day has reached near equilibrium. However, in terms of absolute magnitude of the turbulence Fig. 5 also shows that the months of lowest absolute turbulence -at night and towards the early morning- are the spring and summer months. The reason for this is that the optical turbulence is proportional to the index of refraction fluctuations, which in turn have origin in fractional changes of air temperature. Therefore, in the summer months with higher atmospheric temperatures, the fractional fluctuations are lower and this translates into lowest C_n^2.

So what is best, the afternoon or the morning twilight for MIR astronomy? Based on the findings shown in here, is no doubt that the morning twilight, with a drier atmospheric column (due to the local temperature inversion layer located at altitudes lower than the observatory sites), and colder near surface atmospheric conditions (due to the radiative cooling of the site) which have also allowed the telescope structures to reach their lowest temperature, together with lower near surface turbulence (because of atmospheric temperatures show lower fractional variability), make the morning twilight a great temporal window for astronomical observations in the mid-infrared.

3.3. Would it be possible to predict periods of low PWV?

The atmosphere is highly unsaturated with respect to water vapor, which is limited by the air temperature through energy considerations. Local sources of water vapor, originating from sublimation of snow/ice, and evaporation of surface waters as well as diffusion of water vapor from sub-surface, are to be considered as important sources of humidity at very dry sites. However, the water vapor field is highly dominated by synoptic and mesoscale dynamics, where the location of high and low pressure centers with respect to a site location become very relevant in the advection of wet and or cold air. Therefore, PWV can be forecasted by means of a mesoscale model [10, 11]. PWV in the Hawaiian Islands is strongly influenced by the location of the Hawaiian High pressure center, which could either bring cold and dry air from the northern latitudes, or warm and wet from the southern latitudes, respectively.

How often and for how long do the dry atmospheric conditions remain? This is an important question. Without generalizing, but as a way to show an example of PWV conditions at Mauna Kea we looked at the PWV gathered at the CSO site (with 10 min time resolution) in 2012. With this the nightly median value of PWV was calculated for each day in 2012, results are shown in Fig. 6. This illustrate that dry conditions, with PWV lower than 1 mm, are usual at

Mauna Kea with advection of very dry air (PWV lower than 0.5 mm) that extend for various days. See for instance, the dry conditions at around day 35 (early February), day 80 (second half in March), day 120 (beginning of May) and day 180 (end of June/beginning of July). This helps to illustrate that when dry conditions occur they tend to stay for several days in agreement with conditions controlled by synoptic scale atmospheric conditions. By the same argument the upper plot in Fig. 6 shows various occasions of advection of wet mass air.

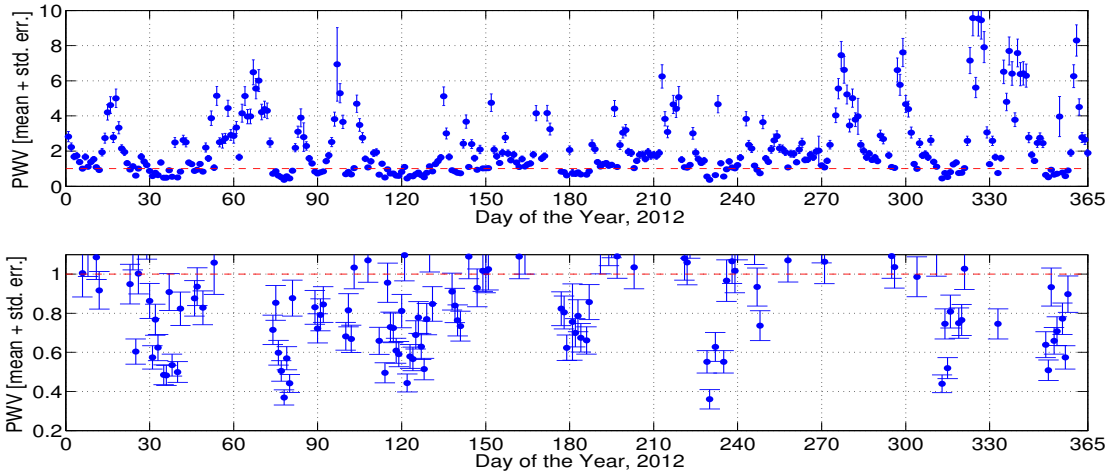

Figure 6. 2012 Nightly mean and its uncertainty of PWV (in mm) at Mauna Kea. The bottom figure limits the vertical scale to 1.1 mm of PWV. The red line shows the 1 mm PWV level and helps as a visual reference to identify all the cases when PWV was lower than 1 mm at the CSO site.

4. Conclusions & Future Work

Astronomical observations in the MIR bands, specially in the Q band, require a dry and cold site to minimize the noise arising from thermal emission of the atmosphere as well as minimize the atmospheric absorption of the astronomical signals. The 13N site, location for the Thirty Meter Telescope, was studied through a site testing campaign effort between 2004 and into 2008. Continuous measurements of PWV have been conducted at the location of the Caltech Submillimeter Observatory for many years. The atmospheric radiance under median conditions of the site in Q band is around 2×10^{-15} W arcsec^{-1} cm^{-2} μm^{-1} and down to less than 10^{-15} W arcsec^{-1} cm^{-2} μm^{-1} in very dry conditions (0.3 mm of PWV). In the N band, the atmospheric radiance get as low as 10^{-17} W arcsec^{-1} cm^{-2} μm^{-1}.

The analysis of site testing data, including temperature and near surface turbulence strength, indicate that optimum conditions are found around morning twilight (between 5:30 AM until 7:30 AM Local Time) when the atmospheric column is usually the driest, colder and more stable. By morning twilight, it is expected that the telescope structures have reached equilibrium with its environment minimizing noise arising from thermal emission scattered from the telescope structures into the mid-infrared detectors.

The atmospheric radiance information, as calculated in this study and shown in Fig. 2 can be used as input for the determination of the thermal emission arriving at the detector of a MIR instrument, a source of noise in the detector. The overall thermal radiance into the detector is a function of, the number of mirrors in the telescope, the optical throughput of the the telescope optics, the thermal emission of the Adaptive Optics instrument, and the quality of the mid-infrared instrument optics. Equation 2, in a generic way, includes the terms relevant for the

determination of the thermal background radiation arriving at the mid-infrared detector), the results in this work can be used to determine that quantity provided all relevant parameters are know.

$$R_{total}(\lambda) = t_{tel}(\lambda) \cdot t_{AO}(\lambda) \cdot t_{midIR}(\lambda) \times Rsky_{total}(\lambda) + t_{AO}(\lambda) \cdot t_{midIR}(\lambda) \times R_{telescope}(\lambda) + t_{midIR}(\lambda) \times R_{AO}(\lambda) + R_{midIRt}(\lambda) \quad (2)$$

Where;

$R_{total}(\lambda)$ is the total thermal background radiation reaching the mid-infrared detector. $t_{tel}(\lambda)$, $t_{AO}(\lambda)$, and $t_{midIR}(\lambda)$ are the optics throughput of the telescope, AO instrument and of the mid-infrared instrument, respectively. $R_{telescope}(\lambda)$ is the thermal emission of the telescope's mirrors, and this can be taken as the summation of each of the mirrors' emissivity multiply by the Planck function at the physical temperature of the mirrors (considered the ambient temperature), i.e. $\epsilon(\lambda) \cdot Planck(\lambda, T)$. Similarly, $R_{AO}(\lambda)$ is the thermal emission from the AO system that goes into the mid-infrared instrument. Finally, $R_{midIR}(\lambda)$ is the internal thermal emission of the mid-infrared instrument itself.

4.1. Acknowledgments

We thank Dr. Simon Radford (Caltech Submillimeter Telescope) for sharing of the 225 GHz tipping radiometer data, and Dr. Hanae Inami (National Optical Astronomy Observatory) for valuables comments regarding science topics of interest for mid-infrared astronomy.

5. References

[1] de Bergh C, Bézard 2003 *Probing Thick Planetary Atmospheres with High Resolution Infrared Spectroscopy* (Proceedings of ESO High Resolution Infrared Spectroscopy in Astronomy Workshop, Springer Science & Business Media) eds H U Käufl, R Siebenmorgen, A F M Morrwood, pp. 514-526.

[2] Kendrew S, Jolissaint L, Brandl B, Lenzen R, Pantin E, Glasse A, Blommaert J, Venema L, Siebenmorgen R, Molster F 2010 *SPIE* **vol. 7735-201**

[3] Lacy J H, Richter M J, Greathouse T K, Jaffe D T & Zhu Q 2002 *Pub. of the Astr. Soc. of the Pac.* **114**, pp.153-168.

[4] Schöck M *et al.* 2009 *Pub. of the Astr. Soc. of the Pac.* **121**, pp.384-395.

[5] Bustos R, Rubio M, Otárola A & Nagar N 2014 *Pub. of the Astr. Soc. of the Pac.* **126**, No 45.

[6] Otárola A *et al.* 2010*Pub. of the Astr. Soc. of the Pac.* **122**, pp.470.

[7] Kataza H, Okamoto Y, Takubo S, Onaka T, Sako S, Nakamura K, Miyata T & Yamashita T 2010 *Proc. SPIE 4008* (Optica and IR Telescope Instrumentation and Detectors) eds M Iye & F M Moorwood.

[8] Seinfield J H & Pandis S N 1998 *Atmospheric Chemistry and Physics* (John Wiley & Sons, New York), pp.1326

[9] Rothman L *et al.* 2008 *J. Quant. Spec. Radiat. Transf.* **110**, pp.533.

[10] Chacón A *et al.* 2011 *Rev. Mex. of A. & A., Serie de Conferencias* **41**, pp.20.

[11] Pozo D *et al.* 2011 *Rev. Mex. of A. & A., Serie de Conferencias* **41**, pp.55.